Soft Matter

COMMUNICATION

View Article Online
View Journal | View Issue

Cite this: *Soft Matter*, 2025, **21**, 2782

Received 22nd January 2025,
Accepted 19th March 2025

DOI: 10.1039/d5sm00074b

rsc.li/soft-matter-journal

Mechanism of microplastic and nanoplastic emission from tire wear†

Shankar Ghosh, *[a] Anit Sane,[a] Smita Gohil,[a] Vedant Vashishtha,[b] Sanat K. Kumar *[c] and Guruswamy Kumaraswamy *[b]

Tire and brake-wear emissions, in particular nanoparticulate aerosols, can potentially impact human health and the environment adversely. While there is considerable phenomenological data on tire wear, the creation and environmental persistence of particulate pollutants is not well understood. Here, we unequivocally show that normal mechanical tire wear results in two distinct micro and nanoplastic (MNP) populations: a smaller, aerosolized fraction (<10 μm), and larger microplastics. Nanoplastic emissions follow a power law distribution that we show is consistent with the classical arguments of Archard, and Griffiths. Nanoplastic pollution increases dramatically with vehicle speed and weight, as the power law distribution characterizing these gets steeper. Charge stabilization of the tire wear nanoparticles keeps them suspended, while microplastics settle due to gravity. Larger microplastics are formed by sequential wear processes and show a log-normal distribution, as anticipated by Kolmogorov. Thus, the particle size distribution provides mechanistic insights to tire fragmentation: the aerosolized fraction is determined by power input to the tire while the larger microplastics are determined by sequential wear processes due to tire-road surface interactions, independent of vehicle weight and speed.

With the ongoing transition to electric vehicles, automotive air pollution will increasingly be dominated by non-exhaust particulate emissions from tire and brake-wear.[1] Recent reports suggest causal links between exposure to particulate pollutants and harmful health outcomes[2–4] and environmental impacts.[5–7] These concerns have prompted several studies characterizing the morphology of tire wear particulate emissions, and the factors that govern these.[8–21] Driving at high speeds or braking abruptly leads to high tire temperatures and the formation of ultrafine tire wear particles formed by the condensation of volatilized organic additives and oils.[16,17] Particle mobility spectrometers report that these ultrafine particles have a monomodal size distribution, centered at a few tens of nanometers.[16–18] Under normal driving conditions, wear of tire tread and brakes results in the formation of micro and nanoplastics (MNPs). Generation of sub-micron to sub-millimeter sized MNPs with either broad monomodal or bimodal distributions has been verified using cascade impactors or optical methods.[8,16–19] There is rising concern about the health and environmental impact of tire wear MNPs, created under normal driving conditions.[8–12,16] Motivated by these observations, here we focus on enunciating the factors that govern tire wear and how these lead to the formation of MNP pollutants, in particular aerosolized fragments, during normal driving conditions.

Tires are complex, highly engineered structures comprising natural or synthetic rubber mixed with nanofillers, that are optimized to maximize road grip and fuel efficiency. An undesirable consequence of frictional road grip is wear of the elastomeric tire tread material when it contacts the pavement. Elastomer wear is determined by viscoelastic processes and by adhesive interactions as it contacts the substrate.[22–24] Thus, the process of tire wear depends on a wide variety of factors, including the type of tire (summer or winter tires), type of pavement (bitumen or concrete) and driving conditions (camber, loading, vehicle speed, acceleration or braking, *etc.*). Previous studies using field measurements or laboratory studies have focused on phenomenological relations between tire wear particles and the factors that control them – rather than on the mechanisms by which the tread wears to generate particles. Determining this critical mechanistic understanding is the focus of the present work.

Field studies to study tire wear particles are complicated by the need to distinguish tyre wear particles from other components of road dust.[14] Road dust could include brake wear particles, fragments from the pavement and even fibers such as wool, cotton that need to be removed by chemical digestion before analysis. These particles confound the analysis since

[a] *DCMP&MS, Tata Institute of Fundamental Research, Homi Bhabha Road, Mumbai, 400005, Maharashtra, India. E-mail: sghosh@tifr.res.in*
[b] *Department of Chemical Engineering, Indian Institute of Bombay, Mumbai, 400076, India. E-mail: guruswamy@iitb.ac.in*
[c] *Department of Chemical Engineering, Columbia University, 500 W 120th St., New York City, USA. E-mail: sk2794@columbia.edu*

† Electronic supplementary information (ESI) available. See DOI: https://doi.org/10.1039/d5sm00074b

they are difficult to distinguish from tyre wear particles. Therefore, model studies using road simulators are carried out, where the tire is abraded against controlled asphalt or concrete-like surfaces that mimic actual road characteristics in terms of roughness and composition. In preliminary experiments where we contacted a tire against an asphalt-like surface, we observed particles from wear of the tire as well as the asphalt. Therefore, we report model experiments where a motor-driven tire is rotated against a freely-rotating aluminium drum. The hard metallic drum does not wear as it contacts the tire, unlike the case of typical pavements. The aluminium drum is cut with grooves running parallel and perpendicular to its axis, to mimic the typical tining of a concrete road.[25,26] These experiments thus allow us to isolate the generation of particles by tire wear from formation of road dust, so that we can focus on the mechanisms by which tire MNPs are generated.

We reasoned that the number distribution of the size of particles generated by mechanical wear under controlled laboratory conditions would provide insight into the mechanisms that govern tread fragmentation. Therefore, we perform measurements on a real tire operating at constant tire speed and constant normal load, respectively, in a series of measurements (see Materials and methods section for details, Fig. S1, ESI†). While there are significant frictional forces at play, we control experimental conditions so that there is only a modest increase in tire temperature relative to the ambient (ranging from 30 to 50 °C, see Materials and methods section, Fig. S2 and Table S1, ESI†) – thus, we are never in a regime where the volatization-condensation mechanism of particle creation is relevant. Further, over this modest range of temperatures, the material properties of the tire tread do not vary substantially so as to alter the physics of the wear process.

The experimental setup is shown schematically and pictorially in Fig. 1. Details of the experimental set-up and protocol are given in the Materials and methods section. There is independent control of the tire speed (through the driving motor) and on the normal force on the tire (by adjusting the center-to-center distance between the axles of the tire and the bottom cylinder). Running the tire for 5 to 10 minutes leads to the creation of a significant number of tire wear particles without significant increase in tire temperature; these MNPs exhibit polydispersity in size and in shape. SEM images of a few particles and a discussion of the shape polydispersity are in the Materials and methods section (Fig. S3, ESI†). We identify the MNP size as the largest characteristic dimension of each particle. We find two distinct populations of wear particles: large particles (typically larger than 100 μm), which settle on a LED panel placed below the tire and are imaged using a Nikon D750 DSLR camera. Smaller particles (0.3 to 10 μm) are aerosolized and are characterized using a particle counter (SPC 8000, Setra). The rate of particle deposition during an experiment increases with the tire speed and the normal force, from $\sim\mathcal{O}(10^3\ \mathrm{s}^{-1})$ for the lowest tire speed and normal load, to $\sim\mathcal{O}(10^4\ \mathrm{s}^{-1})$ for the highest (Materials and methods section, Fig. S4, ESI†). For our choice of experimental conditions, the deposited particles are spatially separated (to facilitate image analysis) we allow sufficient time for particle deposition (at least 5 minutes), and up to 10 min at low v and F_N so that there are sufficient particles (over 5×10^5 particles for each experiment) to provide good statistics for characterizing their size distribution, while limiting the tire temperature to under 50 °C (details in the ESI,† Fig. S5).

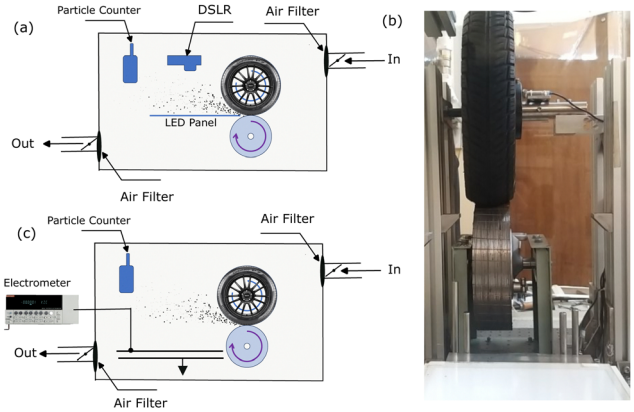

Fig. 1 Schematic depiction of the setup and (a) particle counting and (c) charge measurement setup. A Michelin 90/100 tire (outer diameter = 430 mm and width = 180 mm), mounted on an electric motor, contacts a metallic aluminum drum (outer diameter = 280 mm). The aluminum drum is free to rotate. The motor is mounted on a load cell to measure the normal force on the tire. The tire is pressurized to its rated value of 36 psi. The entire set-up is placed inside a plexiglass chamber, with an arrangement to flush it with filtered air. A 6 channnel aerosol particle counter is mounted within the chamber (top left in the figure). Tire wear particles deposited on a horizontal 0.6 m long LED panel are imaged using a camera.

The resulting size-dependent probability density function (PDF) for MNP sizes are shown in Fig. 2 for two selected velocities

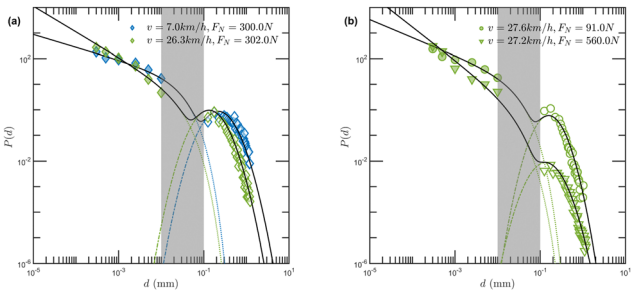

Fig. 2 The probability density function (pdf) for the particles generated is plotted as a function of particle size, d. Filled symbols denote data from the particle counter, while open symbols illustrate data from imaging experiments. Using our current experimental protocol, we are unable to collect data in the size range shown by the gray band. We present data (a) at constant normal force F_N = 300 N, as v is increased from 7 km h^{-1} to 26 km h^{-1} and (b) at constant v = 27 km h^{-1}, as F_N is increased from 91 N to 560 N. A more extensive data set is provided in Fig. S5(b) (ESI†). In all cases, the data fit well with the functional expression $\partial_t n(d) = \frac{A}{d^\alpha}\exp\left(-\frac{d}{d_o}\right) + \frac{B}{d\sigma\sqrt{(2\pi)}}\exp\left(-\frac{\left(\ln\frac{d}{\mu}\right)^2}{2\sigma^2}\right)$, where d_o is associated with the exponential cutoff, and α is the power-law exponent.

and applied forces (data for the entire range of v and F_N is provided in Fig. S5b, ESI†); each of these PDFs are well fit by a two-part function. The aerosolized MNPs characterized using the particle counter (size <10 μm) are fit by a power law with an exponential cutoff, $\propto d^{-\alpha}e^{-d/d_o}$, with a characteristic size of $d_o = 20$ μm. The fit is not sensitive to the chosen d_o in the range of 10–30 μm. While previous studies have reported mono- or bimodal tire wear particle size distributions, the observation of aerosolized particles with a power law distribution is unprecedented. Larger tire wear microplastics that are deposited on the LED panel appear to follow a log-normal distribution with median μ and width σ. This log-normal size distribution is consistent with previous reports of monomodal particle size distributions obtained from tire wear experiments.[18–21] We note that it is possible to obtain reasonable fits to the data over the entire range using only a power-law with a cut-off. This fit is more parsimonious in terms of parameters, but misses data points at the lowest microparticle sizes. Unfortunately, we do not have data in the range of 10–100 μm due to experimental limitations (region indicated in gray in Fig. 2 and Fig. S5b, ESI†). Parenthetically, we comment that the key features that guide our understanding of tire wear particle formation are preserved for both the fits, *viz.* the power law gets steeper for higher v and F_N, while the size of the microplastic fragments (given by the median, mu for the two-part fit, and the power-law cut-off for the parsimonious fit) are largely independent of the experimental conditions. Therefore, our choice of using a two-part function is motivated by more detailed reports in the fragmentation literature.[27–29] Therefore, we proceed with describing the data using a two-part function.

Qualitatively, it appears that the power law characterizing the aerosolized particle distribution gets steeper with increase in speed and with normal load. Thus, the fraction of nanoparticulate pollutants increases significantly with vehicle speed and weight. In contrast, the distribution of the larger tire-wear microplastics appears relatively insensitive to the vehicle speed and weight. To understand the observed phenomenology of MNP creation, we now focus on the physics of fragmenation. For context, we note that fragmentation processes are observed in a wide variety of phenomena, ranging from crushing and grinding mineral ore[27] to breakup of raindrops[30] and formation of volcanic ash.[31] Independent single fragmentation processes lead to the formation of materials characterized by self-similar power-law size distributions, while sequential fragmentation yields a log-normal Weibull distribution.[28,29] Tire wear particles are characterized by smaller MNPs with a power law distribution and larger microplastics with a log normal distribution. This strongly suggests that independent processes lead to the formation of smaller MNPs and larger micro plastic fragments - this has also been seen in rock crushing.[27]

We first consider the size distribution of smaller MNPs that exhibit a power law with an exponential cutoff. For mechanical fragmentation, the fracture length scale sets the distance from the crack tip over which elastic stresses are propagated.[32,33] This can be estimated as $\delta = G_c/E$, where $G_c \sim 100$ J m^{-2},[34] is the strain energy release rate and $E \sim 10$ MPa[35] is the elastic modulus of a typical filled tire tread compound. Thus, $\delta \sim \mathcal{O}(10$ μm), apparently consistent with the d_o values from our fits. Importantly, our estimates for d_o are similar to those found by Persson[36] by fitting literature data to an exponential distribution. The smaller fragments then result from local fragmentation events below this length scale.

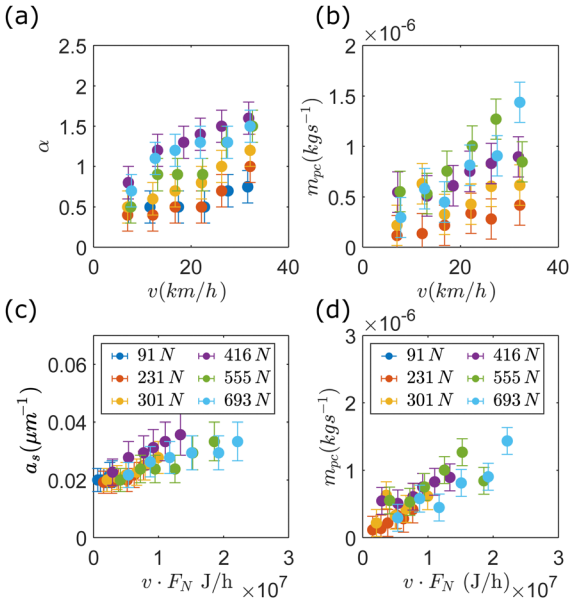

Fig. 3 Variation of α (a) and the total mass m_{pc} (c) of the particles, as measured by the particle counter, are shown as a function of velocity v for different values of the normal force F_N. The specific surface area a_s (b) and m_{pc} (d) for the small MNPs are found to scale with the product of velocity v and normal force F_N.

There is a systematic increase in α, that characterizes the steepness of the power law, with tire speed and normal load (Fig. 3a). Thus, we reiterate that even as the number of tire wear particles systematically increases with tire speed and normal load, there is a significant change in the smaller fragment size distribution while the larger particle size distribution is relatively insensitive to driving conditions. This is an important difference from previous reports[36] that suggested that the tire wear particles follow an exponential distribution. An exponential distribution significantly underestimates the formation of small sized particles, relative to the power law distribution observed in these experiments.

We obtain the total mass production rate, m_{pc} of the smaller MNPs by integrating the aerosol counts across all particle sizes (300 nm $< d <$ 10 μm). The mass, m_{pc}, was calculated assuming the particles are spherical, and that the tire density is 1140 kg m^{-3}.[37] Fig. 3b shows an increase in m_{pc} with the tire velocity, v and normal load, F_N. We note that the large error bars reflect the difficulties associated with making these measurements - thus, while m_{pc} clearly increases from the lowest to highest v and F_N, it difficult to unambiguously claim that the increase in m_{pc} is strictly monotonic due to the large uncertainities associated with this measurement. Archard's law[38] states that the total volume of wear debris scales with the energy input into the system. Extending this idea to our experiments shows that the mass production rate should scale as the frictional

force times the relative velocity between the tire and the drum. The frictional force scales with F_N and we find that the relative velocity scales linearly with the tire velocity (see Materials and methods section, Fig. S9a, ESI†). We observe that plotting m_{pc} as a function of vF_N collapses the data from all our experiments into an approximately linear single trend, consistent with Archard's law (Fig. 3d). For a hardness = 30 MPa, characteristic of filled rubber, we estimate an Archard's law coefficient, $K \approx 10^{-5}$, which is well within the expected range of values.[39]

To understand the origins of the power law exponent, α, we invoke ideas of Griffith[40] and postulate that the energy input into the tire is used to create MNP surfaces. Thus, the surface area created during MNP formation must be proportional to the energy input into the tire, *i.e.*, vF_N. Since the m_{pc} increases linearly with the energy input, the mean specific surface area for the small MNPs, $a_s = \frac{\int_0^\infty r^{2-\alpha} e^{-r/d_o} dr}{\int_0^\infty r^{3-\alpha} e^{-r/d_o} dr} = \frac{1}{d_o} \frac{\Gamma(3-\alpha)}{\Gamma(4-\alpha)}$ should be independent of vF_N. While Fig. 3c show a superposition for the α data at different v and F_N, it is evident that a_s has a weak dependence on vF_N. We note that our calculation of m_{pc} and a_s assumes that tyre wear particles are spherical. However, images of the particles show a clear deviation from a spherical shape (ESI,† Fig. S3), with systematic increase in eccentricity for higher v and F_N (ESI,† Fig. S4). The microscopic images provide a 2D projection of the particles – however, if we assume that the particles show uniaxial symmetry, it is possible that the a_s estimated for ellipsoidal particles will be independent of v and F_N. Alternately, it is well understood in the fracture literature that the Griffith model accounts only for the creation of new surfaces due to energy input, but does not account for viscoelastic loss. Therefore, it is possible that a more complete theory that accounts for these viscoelastic terms might better describe the relatively modest dependence of a_s on vF_N observed in our data.

We now examine the size distribution of the larger MNPs. The median, μ, and width, σ, that characterize the log-normal distribution exhibit only relatively modest variations with the tire velocity and normal force, F_N (see Materials and methods section, Fig. S6, ESI†). We note that fits to μ and σ are characterized by large error bars since we do not have good data at the lower end of the distribution. Additionally the data at the lowest v and F_N are noisy. Therefore, within these constraints, we cannot make any additional comments beyond stating that there is no signification variation in μ and σ over this range of v and F_N. Interestingly, these values are of the order of the groove depth on the metal drum (1 mm). We, therefore, believe that the specifics of the larger MNP distribution reflects the geometry of the road. Further support for this conjecture was obtained by using a drum with different groove geometry (horizontal grooves with a depth of 0.5 mm). For these experiments, the maximum value of the particle size distribution shifted to smaller values (see Materials and methods section, Fig. S7, ESI†). Our results are consistent with previous studies[41–44] that indicate that the size of particles resulting from tire wear is determined by the roughness of the road and the nominal maximum aggregate size. Regardless, the fact that the larger microparticles are described by a log normal size distribution implies that these pollutants form through sequential fragmentation, as has been proposed in general arguments by Kolmogorov.[45]

We observe that the aerosolized MNP concentration decreases once the tire stops rotating (Fig. S5, ESI†), with a time scale determined by the particle size. Counts for the 300 nm sized particles do not return to the baseline value even after several hours, implying that they do not agglomerate and remain suspended for an extended time scale. We propose that the smaller MNPs remain suspended as a result of electrostatic stabilization. Larger tire wear particles do not stay suspended and settle, with the counts for the 10 μm channel returning to the baseline value within a few seconds. In addition to gravitational settling, the decrease in the particle counts also arises from charge-mediated adsorption of MNPs on the walls of the plexiglass container. The application of a positive electrostatic pulse to the plexiglass walls resulted in rapid desorption of MNPs and a corresponding increase in aerosolized particle counts. Clearly, the adsorbed MNPs are negatively charged. To provide more credence to this picture, we measured the charge on large MNPs that settle on the bottom plate (methods described in Materials and methods section). These MNPs (Fig. S8, ESI†) are also negatively charged. The total charge normalized by MNP mass grows linearly with the tire speed, and is relatively insensitive to the normal force. We note that a recent study reported that brake wear particles are highly charged, and that charging characteristics are dependent on the brake pad material.[46]

Thus, the mechanical fragmentation of tires results in small MNPs (sizes $\leq$10 μm) with a power law distribution and larger MNPs with a log normal distribution. Increases in tire velocity and in normal force result in an increase in the number of small particles emitted. Therefore, there is an increase in primary fragmentation of tire tread for vehicles that are driven faster or that are heavier. Since these particles are charge-stabilized, they can persist in the atmosphere and thus have the potential to significantly affect atmospheric PM1 and PM2.5 counts with deleterious consequences on health and the environment. We note that recent proposals to regulate automotive non-exhaust emissions seek to place limits on PM10.[47] Smaller environmentally persistent nanoplastics are likely underrepresented in PM10, compared with larger ($\approx$10 μm) microplastics that exhibit gravitational settling. Moreover, given that the size distribution of small MNPs follows a scale-independent power law form, it is unlikely that they can be mitigated by changing material properties alone. However, from an optimistic viewpoint, their charged character makes it possible to capture these particles near the tire itself using, for example, electrostatic precipitators. This strategy could prevent their aerosolization and thus mitigate these atmospheric pollutants.

Data availability

The data supporting this article have been included in the main manuscript and in the ESI.†

Conflicts of interest

There are no conflicts to declare.

Acknowledgements

SKK graciously acknowledges funding from NSF award DMR-2301348

References

1 V. R. Timmers and P. A. Achten, *Atmos. Environ.*, 2016, **134**, 10–17.
2 Z. Tian, H. Zhao, K. T. Peter, M. Gonzalez, J. Wetzel, C. Wu, X. Hu, J. Prat, E. Mudrock and R. Hettinger, *et al.*, *Science*, 2021, **371**, 185–189.
3 W. Hill, E. L. Lim, C. E. Weeden, C. Lee, M. Augustine, K. Chen, F.-C. Kuan, F. Marongiu, E. J. Evans Jr and D. A. Moore, *et al.*, *Nature*, 2023, **616**, 159–167.
4 C. A. PopeIII, R. T. Burnett, M. J. Thun, E. E. Calle, D. Krewski, K. Ito and G. D. Thurston, *JAMA*, 2002, **287**, 1132–1141.
5 L. E. Revell, P. Kuma, E. C. Le Ru, W. R. Somerville and S. Gaw, *Nature*, 2021, **598**, 462–467.
6 J. Brahney, N. Mahowald, M. Prank, G. Cornwell, Z. Klimont, H. Matsui and K. A. Prather, *Proc. Natl. Acad. Sci. U. S. A.*, 2021, **118**, e2020719118.
7 N. Evangeliou, H. Grythe, Z. Klimont, C. Heyes, S. Eckhardt, S. Lopez-Aparicio and A. Stohl, *Nat. Commun.*, 2020, **11**, 3381.
8 D. Kaul and M. Sharma, *et al.*, *Atmos. Environ.*, 2009, **43**, 5691–5697.
9 M. Mathissen, J. Grochowicz, C. Schmidt, R. Vogt, F. H. F. zum Hagen, T. Grabiec, H. Steven and T. Grigoratos, *Wear*, 2018, **414**, 219–226.
10 M.-J. Foitzik, H.-J. Unrau, F. Gauterin, J. Dörnhöfer and T. Koch, *Wear*, 2018, **394**, 87–95.
11 I. Park, H. Kim and S. Lee, *J. Aerosol Sci.*, 2018, **124**, 30–40.
12 A. E. Thomas, P. S. Bauer, M. Dam, V. Perraud, L. M. Wingen and J. N. Smith, *Proc. Natl. Acad. Sci. U. S. A.*, 2024, **121**, e2313897121.
13 B. Baensch-Baltruschat, B. Kocher, F. Stock and G. Reifferscheid, *Sci. Total Environ.*, 2020, **733**, 137823.
14 L. J. Knight, F. N. Parker-Jurd, M. Al-Sid-Cheikh and R. C. Thompson, *Environ. Sci. Pollut. Res.*, 2020, **27**, 18345–18354.
15 J.-h Kwak, H. Kim, J. Lee and S. Lee, *Sci. Total Environ.*, 2013, **458**, 273–282.
16 A. Dahl, A. Gharibi, E. Swietlicki, A. Gudmundsson, M. Bohgard, A. Ljungman, G. Blomqvist and M. Gustafsson, *Atmos. Environ.*, 2006, **40**, 1314–1323.
17 I. Park, J. Lee and S. Lee, *Aerosol Sci. Technol.*, 2017, **51**, 188–197.
18 M. Gustafsson, G. Blomqvist, A. Gudmundsson, A. Dahl, E. Swietlicki, M. Bohgard, J. Lindbom and A. Ljungman, *Sci. Total Environ.*, 2008, **393**, 226–240.
19 M. L. Kreider, J. M. Panko, B. L. McAtee, L. I. Sweet and B. L. Finley, *Sci. Total Environ.*, 2010, **408**, 652–659.
20 J. M. Panko, K. M. Hitchcock, G. W. Fuller and D. Green, *Atmosphere*, 2019, **10**, 99.
21 M. Mathissen, V. Scheer, R. Vogt and T. Benter, *Atmos. Environ.*, 2011, **45**, 6172–6179.
22 A. Schallamach, *Wear*, 1958, **1**, 384–417.
23 Y. Fukahori, P. Gabriel and J. Busfield, *Wear*, 2010, **269**, 854–866.
24 H. Liang, Y. Fukahori, A. Thomas and J. Busfield, *Wear*, 2009, **266**, 288–296.
25 M. B. Snyder, *et al.*, Concrete Pavement Texturing, United states. federal highway administration. **https://www.fhwa.dot.gov/pavement/pubs/hif17011.pdf** technical report, 2019.
26 The Standard Specifications for the Construction of Roads and Bridges on Federal Highway Projects, US Dept. of Transportation; **https://highways.dot.gov/federal-lands/specs#:text=Standard**.
27 R. King, *Int. J. Miner. Process.*, 1979, **6**, 207–220.
28 W. K. Brown and K. H. Wohletz, *J. Appl. Phys.*, 1995, **78**, 2758–2763.
29 P. Rosin and E. Rammler, *Kolloid-Z.*, 1934, **67**, 16–26.
30 E. Villermaux and B. Bossa, *Nat. Phys.*, 2009, **5**, 697–702.
31 E. Kaminski and C. Jaupart, *J. Geophys. Res.:Solid Earth*, 1998, **103**, 29759–29779.
32 C. W. Barney, I. Sacligil, G. N. Tew and A. J. Crosby, *Soft Matter*, 2022, **18**, 4220–4226.
33 R. Long, C.-Y. Hui, J. P. Gong and E. Bouchbinder, *Annu. Rev. Condens. Matter Phys.*, 2021, **12**, 71–94.
34 G. J. Lake and A. G. Thomas, *Proc. R. Soc. London, Ser. A*, 1967, **300**, 108–119.
35 B. Lorenz, B. Persson, G. Fortunato, M. Giustiniano and F. Baldoni, *J. Phys.: Condens. Matter*, 2013, **25**, 095007.
36 B. Persson, *J. Phys.: Condens. Matter*, 2009, **21**, 485001.
37 H. Parung, R. Irmawaty and D. Wijaya, *IOP Conf. Ser.: Earth Environ. Sci.*, 2020, 012068.
38 A. Zmitrowicz, *J. Mec. Theor. Appl.*, 2006, **44**, 219–253.
39 J. Archard, *J. Appl. Phys.*, 1953, **24**, 981–988.
40 A. A. Griffith, *Philos. Trans. R. Soc., A*, 1921, **221**, 163–198.
41 J. Lee, O. Kwon, Y. Hwang and G. Yeon, *Appl. Sci.*, 2024, **14**, 6362.
42 A. Veith, *The Tire Pavement Interface*, ASTM International, 1986.
43 S.-H. Bae, E. Chae, Y.-S. Park, S.-W. Lee, J.-H. Yun and S.-S. Choi, *Sci. Total Environ.*, 2024, **944**, 173948.
44 J. O. Allen, O. Alexandrova and K. E. Kaloush, *et al.*, Arizona. Dept. of Transportation, 2006, Report submitted to Arizona Department of Transportation (Contract KR-04-0720-TRN), **https://azdot.gov/sites/default/files/2019/05/tire-wear-emissions-for-asphalt-rubber-portland-cement-concrete-April2006.pdf**.
45 S. Redner, in *Statistical Models for the Fracture of Disordered Media*, ed. H. J. Herrmann and S. Roux, North-Holland, Amsterdam, 1990, pp. 321–348.
46 A. E. Thomas, P. S. Bauer, M. Dam, V. Perraud, L. M. Wingen and J. N. Smith, *Proc. Natl. Acad. Sci. U. S. A.*, 2024, **121**, e2313897121.
47 European Motor Vehicles Emissions Regulations, 2022, **https://eur-lex.europa.eu/legal-content/EN/TXT/**? uri = CELEX:52022PC0586, accessed on December 10, 2024.

